Sustainable Energy Technologies and Assessments 45 (2021) 101085

Contents lists available at ScienceDirect

Sustainable Energy Technologies and Assessments

journal homepage: www.elsevier.com/locate/seta

Original article

Very short-term temperature forecaster using MLP and N-nearest stations for calculating key control parameters in solar photovoltaic generation

Fermín Rodríguez [a,b,*], Michael Genn [c], Luis Fontán [a,b], Ainhoa Galarza [a,b]

[a] Ceit-Basque Research and Technology Alliance (BRTA), Manuel Lardizabal 15, 20018 Donostia/San Sebastián, Spain
[b] Universidad de Navarra, Tecnun, Manuel Lardizabal 13, 20018 Donostia/San Sebastián, Spain
[c] Griffith University, 170 Kessels Road, Nathan, QLD, Australia

ARTICLE INFO

Keywords:
Solar photovoltaic generation
Smart grid
Neural networks
Very short-term temperature forecaster

ABSTRACT

Although photovoltaic generation has been proposed as a solution for the world's energy challenges, it depends to a large extent on solar irradiation and air temperature. Therefore, small variations in these meteorological parameters produce sudden changes in power generation, which makes it difficult to integrate photovoltaic generators into the electrical grid. The aim of this study is to develop a very short-term temperature forecaster that makes photovoltaic generation more reliable in order to provide not only power but also ancillary services. To predict ambient temperature in a specific area (Vitoria-Gasteiz, Basque Country) in the next 10 min, this forecaster combines a multilayer perceptron and the optimal nearest number of meteorological. In addition, the distance and relative location between each station and the target station were taken into account. The accumulated deviation between actual and forecasted temperature was lower than 1% in 96.60% of the examined days from the validation database. Moreover, the root mean square error was 0.2557 °C, which represents an improvement of 13.20% as compared with the benchmark result. The results indicated that the forecaster can be considered for implementation in photovoltaic generators to compute key control parameters and improve their integration into the electrical grid.

Introduction

Electrical power has been at the heart of the socio-economic development of modern countries, and it is expected that its relevance will continue in the near future due to the high number of everyday devices that require electricity, such as electric vehicles and household equipment [1,2]. Traditionally, technologies based on fossil resources have been the most commonly used for electricity generation, but these technologies have drawbacks, such as low efficiency in the electricity generation process [3] as well as the fluctuation of fossil fuel prices [4], the greenhouse effect and CO_2 emissions [5]. Because of the combustion that takes place in non-renewable power generation technologies, the different types of pollutants that transfer to the atmosphere and radioactive waste may need to be managed. Furthermore, societies and governments are becoming aware of the negative effects of non-renewable technologies [6] and the need for a gradual transition to achieve the goal of a fully renewable generation system [7].

Different renewable technologies—such as hydro, solar thermal, solar photovoltaic (PV), wind, geothermal—have been proposed in recent decades, and some of them have developed quickly due to advantages such as easy installation or high efficiency. For instance, solar photovoltaic and wind generators have experienced significant improvement, and the number of generators based on these technologies are on the rise [8]. The main reasons for this rise in the installed power of these renewables are the abundance of solar irradiation and windy locations, as well as their easy integration for both large-scale generators and small-scale self-supply installations [9,10]. However, if increasing the number of large and small renewable generators connected to the traditional network is the objective, challenges such as the intermittent nature of renewables and location dependence need to be addressed [11].

To reliably operate power systems, accurate forecasting of the power produced by renewables and the power demanded by the loads is needed. Many decisions related to the energy sector, such as real-time dispatch, unit commitment, economic dispatch and maintenance planning, depend on the value of different time horizon forecasters [12]. In addition, the European Commission [13] and the International Renewable Energy Agency [14,15], through different roadmaps and in official reports, have started proposing scenarios where the renewable energy

* Corresponding author at: Ceit-Basque Research and Technology Alliance (BRTA), Manuel Lardizabal 15, 20018 Donostia/San Sebastián, Spain.
E-mail address: frlalanne@ceit.es (F. Rodríguez).

https://doi.org/10.1016/j.seta.2021.101085
Received 10 August 2020; Received in revised form 5 January 2021; Accepted 30 January 2021
Available online 26 February 2021

Nomenclature

t	Current time
h	Forecast horizon
i = 1, 2…, N	Examined number of samples
I_{SC}	Short-circuit current (A)
P_m	Generated output power (W)
RMSE	Root Mean Square Error (°C)
R^2	R-squared
V_{oc}	Open voltage circuit
Y_i	Actual value
$Y_i^{'}$	Forecasted value
$\overline{Y}$	Mean value of the analysed forecasts
AC	Alternating Current
ANN	Artificial Neural Network
ISDA	Iterative Single Data Algorithm
MLP	Multilayer Perceptron
PV	Photovoltaic
RNN	Recurrent Neural Network
SMO	Sequential Minimal Optimisation
SVM	Support Vector Machine

generators can also offer certain ancillary services, which comprise a wide variety of operations that support and control the power flow from generators to consumers and maintain the grid's reliability, stability and security.

Traditionally, synchronous generators connected directly to the AC grid were responsible for providing ancillary services, such as maintaining the main grid's frequency and voltage levels [16,17]. Although in the new scenario, renewable generators will be allowed to provide some ancillary services, depending on the country, different types of penalties can be imposed when ancillary service sellers fail to provide their service [18]. Therefore, if a higher penetration of new renewable generators is desired to increase the installed green power capacity as well as provide ancillary services, it is fundamental that the uncertainty of green technologies be reduced by developing more accurate forecasters. Frequency regulation, load following, operating reserve, reactive power support and black start services are the ancillary services that are expected to be provided by the green technologies such as hydro, wind or PV plants in the near future [18].

An analysis of the current literature related to the development of forecasters showed that researchers categorise forecasters according to horizon time. As a consequence, forecasters are usually classified in the following categories [19]:

- **Very Short-Term Forecast:** In this category, the forecasters make predictions some minutes in advance. Forecasted values are used for the real-time dispatch of different scale power systems [20,21].
- **Short-Term Forecast:** These forecasters predict for a range of time, going from a few hours to a day ahead, and the predicted parameters are used to make decisions about things such as unit commitment or economic dispatch [22,23].
- **Medium-Term and Long-Term Forecast:** The forecasters provide information from a day to a few weeks ahead and from a few weeks to months ahead, respectively. These forecasters predict information regarding future power demand and the results are used for maintenance activities [24,25].

Solar generation technologies have evolved greatly in recent years and solar power plant capacity has also expanded, and this development and penetration trend is expected to continue into the future [8,26]. However, to ensure the quick integration of these generators into the traditional network, the accuracy of the monitorisation and prediction tools must be improved. Following the proposal by Elsinga et al. [19], if the desire is to increase photovoltaics' ability to reliably provide ancillary services like frequency regulation, operating reserve or black start services, it is necessary to improve their control. In addition, accurate forecasters for prediction horizons smaller than 15 min are needed to achieve this goal. Due to the fact that the available databases have sampling times of 10 min, the shortest prediction horizon that can be developed through these databases without modifying the recorded data also needs to be a 10-minute prediction horizon.

In solar generation, there are three key parameters that must be monitored and computed in order to develop a proper control strategy: solar irradiation, cell temperature and power output [2]. In addition, the last two parameters are also affected by wind speed [2,27] and ambient temperature [2,28], as has been demonstrated by a variety of studies. Although solar irradiation prediction [20,21] and cell temperature estimation [27,28] have been widely researched due to their direct impact on power generation and control strategies, other parameters have been studied less due to their lower or indirect impact; one such parameter is ambient temperature forecasting [29].

Very short-term temperature forecasters have traditionally been developed to provide information for other variables, such as the management of devices for energy savings in buildings [30], as input for energy demand prediction algorithms [31,32] or for solar irradiation forecasting [33]. However, a search of the literature did not yield many analyses of the benefits of temperature prediction on solar photovoltaics' key control parameters and power generation. Furthermore, the literature review shows that in recent years more sophisticated techniques have been developed in order to improve the accuracy of temperature forecasters.

In the literature, the vast majority of the forecasters developed for predicting meteorological parameters can be classified into physical models or statistical methods. While physical models rely on a set of equations to describe physical phenomena and predict future weather variables [23,34], statistical methods rely on time-series forecasting throughout the use of historical databases [29,35]. For instance, Mba et al. [36] and Li et al. [37] proposed an artificial neural network and an Elman multistep network approach, respectively, for indoor temperature predictions in the short-term. While a correlation coefficient of 0.985 was obtained through the forecaster presented by [36], the error metrics calculated in [37] were near zero. However, other authors, such as Li et al. [38], have presented support vector machine techniques as an alternative to indoor temperature hour-ahead forecast and with a root mean square error metric range between 0.006 and 1.182.

This study focuses on the analysis of the best statistical technique for developing a very short-term outdoor temperature forecaster, due to the complex implementation of physical models and the good forecast results obtained by statistical techniques for indoor temperature forecast. The tool developed merges artificial intelligence and the optimal number of nearest meteorological stations to forecast temperature in the location where the photovoltaic panels are set. Therefore, it will be possible to compute photovoltaics' characteristic parameters, such as cell temperature (T_c), open voltage circuit (V_{oc}) and output power (P_m), making them more reliable not only for providing power supply but also ancillary services.

To design the final structure of the forecaster, different combinations of strategies/methods and iterative processes were applied. Therefore, the article provides the most important information from each step. The key contributions of this study are as follows:

1) A very short-term air temperature forecaster was developed in order to integrate it into solar photovoltaic generators and compute their key control parameters. The forecaster, which is based on the combination of a multilayer perceptron and the optimal number of nearest meteorological stations, will help to improve the control strategy of solar generators. Because the available data is limited, the

temperature forecasting model was developed for a specific area, Vitoria-Gasteiz, Basque Country.
2) The input parameters used in the forecaster to make the predictions are: season, time, the distance and relative position between the target stations and the selected stations, and the air temperature of target and selected stations in the last 24 h, whereas the forecaster's output is temperature prediction 10 min ahead.
3) Because there is not much literature related to air temperature forecasters for solar photovoltaic control parameter computation, to develop our forecaster different prediction methods were tested to select the method that produces the lowest root mean square error and highest R-squared error metrics. Moreover, root mean square error and R-squared were used, to compare actual and forecasted values not only with the methods developed but also with the results provided in the literature.
4) Through the developed forecaster, cell temperature (T_c), open voltage circuit (V_{oc}) and output power (P_m), the characteristic parameters of photovoltaic generation can be computed. This will make it possible to introduce both small and large-scale generators in current electrical grids, allowing them to not only produce power but also provide ancillary services to the main grid, maximising the renewable generator's profits. This increase in renewables will lead to a cleaner generation mix, a reduction of the whole system's cost due to the lower generation cost of the renewables, and a reduction in CO_2 emissions.

The remaining sections of the article are organised as follows: Section 2 analyses different models for temperature forecasting and explains the proposed model, Section 3 presents the results obtained through these models and compares the results provided in the literature, and Section 4 presents the conclusions of this study.

Temperature forecasting algorithms

Examined techniques

After reviewing the literature, it was concluded that few studies have examined outdoor temperature forecasting for short-term horizons [2,29,31,39]. It must be taken into account that temperature affects socio-economic activities; this is the reason why the vast majority of the existing forecasters are for longer prediction horizons than the forecast horizon that we are developing in this study in order to improve photovoltaic control strategy. The techniques we analysed to develop a 10-minute-in-advance forecaster were the persistence method, artificial neural networks (ANNs) and support vector machines (SVMs). The persistence method was chosen because it is easy to implement and it is commonly used as a benchmark to analyse the improvement of new forecasters [20,21]. With respect to the ANN and SVM techniques, these have been able to forecast indoor temperature with high accuracy for other goals and longer prediction horizons [31,39]. Therefore, both were examined in order to determine whether they were able to predict outdoor temperature for the stated forecast horizon.

Persistence method

A persistence model is a very short-term forecasting technique that is easy to programme and often used as a benchmark to compare more complex forecast methods [31]. The assumption behind this technique relies on the fact that little to no change will occur between the current moment and prediction moment.

Therefore, the predicted value for the chosen forecast horizon is equal to the last measured value.

$$F(t+h) = F(t) \tag{1}$$

where $F(t+h)$is the forecasted value for a forecast horizon time of h and $F(t)$is the current value of the forecast parameter.

Meteorological data is highly autocorrelated due to the fact that data recording is done from adjacent points in time [40]. This means that for short forecast horizons, the correlation between current and future value increases. Hence, the persistence model is able to predict with sufficient accuracy. However, this technique lags one step behind the actual value of the meteorological parameter. Therefore, its accuracy decreases when sudden changes occur and/or when the forecast horizon increases.

Artificial neural network (ANN) methods

The strength of ANNs as classifying and regression tools is due to their ability to generalise and produce reasonable outputs from data that has never been seen before [41,42]. In addition, ANNs' capability to model non-linear processes throughout non-linear activation functions and the development of supervised learning algorithms have resulted in considerable success for ANNs [43]. This capability and development have led to ANNs being applied in different fields, such as solar irradiation [44] and wind speed forecasting [45]. ANNs can be classified as recurrent neural networks (RNNs) and multilayer perceptrons (MLPs); both were analysed in this study. After reviewing the available literature [36,46], we decided that MLP and RNN architectures would have only a single hidden layer. In addition, Panchal et al. [47] concluded that developing architectures with two hidden layers almost never improves a forecaster's accuracy but increases the risk of converging into a local minimum.

Recurrent neural networks. The main characteristic of RNNs is the incorporation of feedback loops. The feedback goes from the output of the intermediate hidden layers back to the input layer of the network. The feedback process requires a time delay function (z^{-s}), which introduces a delay of 's' steps, and for each step the delayed output state of the hidden layer is introduced, along with new input data for the input of the network. The introduction of feedback loops increases the learning capability of the forecaster and usually produces more accurate forecasts [43].

Multilayer perceptron networks. The easiest and most common implementation of ANNs is a fully connected MLP. The principal components of a MLP are artificial neurons. These neurons, which are located in the layers of the network, are connected through synaptic weights and exhibit nonlinear behaviour. The neurons' behaviour is mathematically expressed the following equations,

$$u_k = \sum_{j=1}^{m} w_{kj} x_j \tag{2}$$

$$y_k = \varphi(u_k + b_k) \tag{3}$$

where x_j is related to the inputs of each neuron and is multiplied by synaptic weight w_{kj}, which expresses the connection strength between two neurons. The result of Eq. (2), u_k, is added to the bias b_k, and that sum is multiplied by activation functionφ to calculate the output valuey_k (see Eq. (3)). This outputy_k is used as input in the following neuron of the network. The bias b_k and synaptic weight w_{kj} parameters are fit in the training step in order to do forecasts with previously unseen inputs. More information about MLPs can be found in [43].

In this configuration, calculations flow in one direction from the input to the output (forward propagation). The benefits of a MLP are: quicker implementation, fast training, robustness to outliers and/or missing data; moreover, when an MLP is designed with an appropriate number of neurons, it is a universal approximator [42,43].

Support vector Machine (SVM) methods

A SVM is a nonparametric technique that can be used for different purposes, such as regression or data classification [48]. To develop a very short-term temperature forecaster, the regression variant of the SVM technique has to be used. A regression SVM is similarly

implemented for an ANN: a set of input values are transformed, through kernel functions, to generate forecast values. The nonparametric nature of SVMs enables the model to vary the number of parameters used during the fitting step, whereas for ANNs all parameters are predetermined [42].

For meteorological forecasting, the inputs are the historical observations recorded from different sensors and the output is the forecasted value for the chosen horizon. SVMs can use different kernel functions to fit an equation that reduces the residual of the forecast; i.e. the difference between the predicted value and the actual value. In addition, while kernel functions will make it possible to converge on a single solution no matter how complicated the problem is [39], other models can converge to a local minimum.

Regarding the convergence control of the SVM technique, there are two key parameters that stand out: ε, which is related to the tolerance for error, and β, which determines the flattest possible solution. Eq. (4) shows the verification that needs to be satisfied when the method is being programmed.

$$\forall n : |g_n - (\dot{x_n}\beta + b)| \leq \varepsilon \quad (4)$$

where ∀n means 'for all n values', g_n is the target value and '$\dot{x_n}\beta + b$' is the regression output of the SVM.

When provided with an adequate database, the SVM regression technique is able to generalise trends and fit an equation within tolerances. However, the optimisation of a given problem with an SVM is not straightforward when huge databases are used. Therefore, it is important to select a suitable kernel function and optimisation algorithm; incorrectly selecting these functions and algorithms increases the probability of convergence on an unsuitable local minimum [39].

N-nearest station model

To develop the model proposed in this study, the N-nearest station model, several steps were carried out. Firstly, one of the forecasting techniques described above was chosen. To that end, several tests were run with these forecasters in the target location in order to select the optimal technique, and the forecaster with lowest RMSE and highest R-squared error metrics was chosen. Secondly, it was necessary to prepare a database with the available stations around the target location, along with the coordinates and recorded temperature measurements for each. Thirdly, the technique chosen in the first step was combined with the database generated in step two. Finally, we empirically determined the number of N-nearest meteorological stations that maximises the accuracy of the proposed forecaster. The flowchart in Fig. 1 illustrates the methodology used to develop our temperature forecaster.

While other models such as numerical weather prediction or satellite imagery need to take into account other meteorological or orographic parameters in order to be able to make accurate forecasts, the N-nearest station model only needs the temperature datasets of the available locations around the target station. The model by itself establishes the relationships between the target and chosen stations that maximise the accuracy of the forecaster.

In Fig. 2, a solid black square marks the target station, which is located in Vitoria-Gasteiz, in the Basque Country, and whose recorded meteorological data was used for the forecaster developed in this study. The white circles represent other stations near the target one, and their databases were also used to develop the proposed forecaster.

Through this model it will be possible to check whether the accuracy of the forecaster selected from among the ones examined in Section 2.1 improves when the optimal number of nearest stations is taken into account when making predictions for the target station. Moreover, each

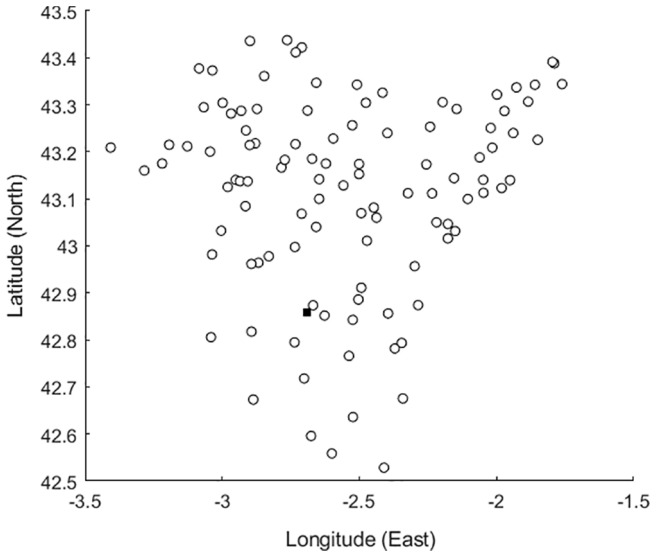

Fig. 2. Distribution of target (solid black square) and available meteorological stations (white circles).

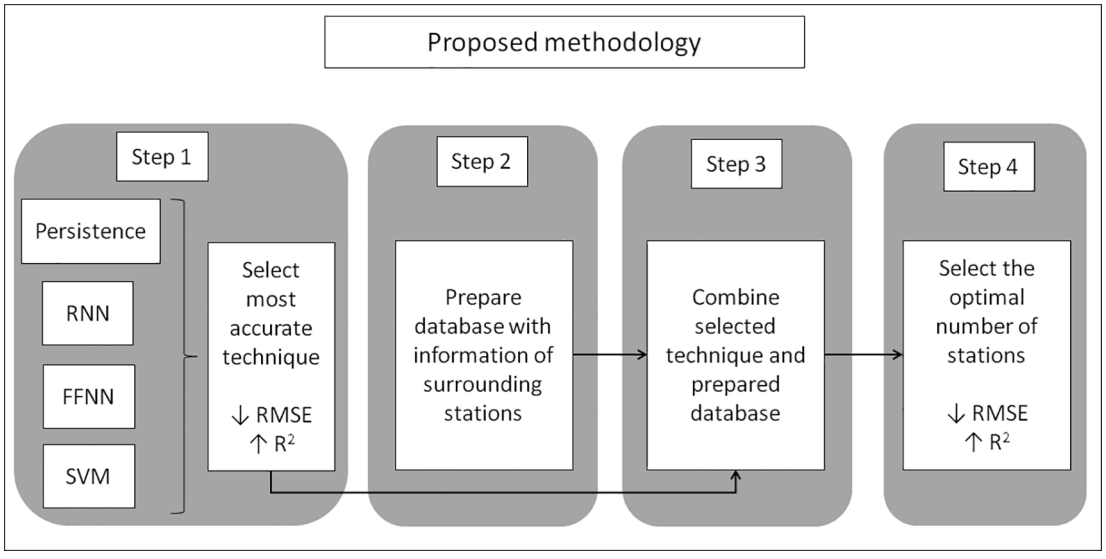

Fig. 1. The main steps in the proposed methodology for developing the N-nearest stations forecaster.

station is going to take into account not only the measurements recorded by the sensors in that station, but also the distance and the relative position between each station and the location where the forecast takes place.

Error metrics

Several error metrics are used in the literature [29,39] to examine the accuracy of newly developed forecasters. In order to be able to make comparisons not only between the programmed models but also with the results provided in the literature, root mean square error (RMSE) and coefficient of determination, also denoted as R-squared (R^2), were chosen. Both metrics analyse the deviation between actual and predicted values.

RMSE and R^2 are defined as:

$$RMSE = \sqrt{\frac{1}{N}\sum_{i=1}^{N}\left(Y_i - Y_i^{'}\right)^2} \tag{5}$$

$$R^2 = 1 - \frac{\sum_{i=1}^{N}\left(Y_i - Y_i^{'}\right)^2}{\sum_{i=1}^{N}\left(Y_i - \overline{Y}\right)^2} \tag{6}$$

where Y_i is the actual value; $Y_i^{'}$is the forecasted value, $\overline{Y}$ is the mean value of the analysed forecasts and N is related to the number of predictions that are analysed over a period of time.

Results and discussion

For this study the meteorological database from Euskalmet, the Basque Meteorological Agency, was used (http://www.euskalmet.euskadi.eus/). The data from the 'C040 Vitoria-Gasteiz' station was downloaded in order to analyse which of the algorithms described in Section 2 was most accurate for temperature forecasting in very short time horizons. In this study, all the models developed were trained with a database from January 2015 to December 2016 and validated with an entire year's data from 2017. The models tested were persistence, recurrent neural network, multilayer perceptron and regression SVM, and all were developed in MATLAB®.

Persistence model (benchmark)

The RMSEs obtained through the persistence model for the training and validation datasets were 0.2916 °C and 0.2996 °C, respectively. These values were used as a benchmark for calculating the 'relative percentage improvement' given by Eq. (7).

$$\text{Improvment}(\%) = \frac{RMSE_{persistence} - RMSE_{method}}{RMSE_{persistence}} * 100 \tag{7}$$

where $RMSE_{persistence}$ pertains to the value obtained by the persistence technique and $RMSE_{method}$ pertains to the value to be compared. The value obtained from Eq. (7) allows the RMSEs obtained through different models to be compared against a reference benchmark, and this value is an intuitive indicator of the forecasting capabilities of the methods studied. Fig. 3 presents a comparison between the actual measurements and those obtained through the persistence model for sample day January 20, 2017.

As expected from the persistence model, the prediction curve is equal to the actual one but delayed one time step. It must be remembered that this model assumes that the predicted value for the chosen forecast horizon is equal to the last measured value; see Eq. (1).

Recurrent neural network

As no analytical methodology for fixing the structure of an RNN was found in the literature, an iterative method was chosen. In addition, to minimise the effect of random initialisation of the network created with MATLAB®, each structure was run five times and the results were averaged [44]. The Levenberg-Marquardt algorithm was applied in the training step due to its robustness and the accurate results achieved in other forecasters [49,50,51].

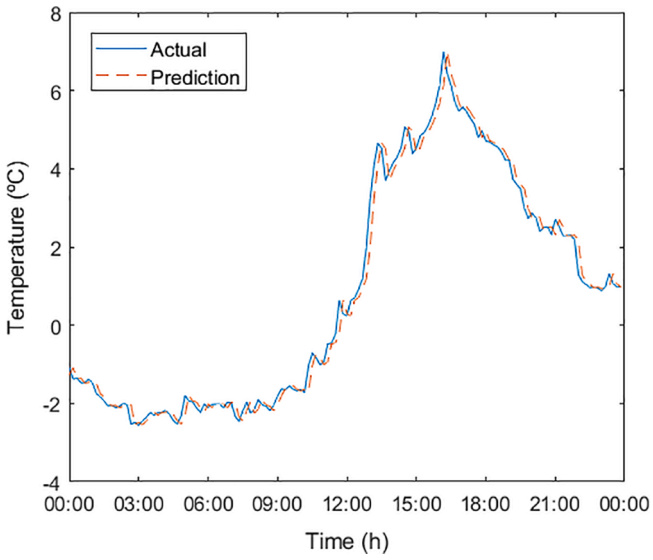

Fig. 3. Actual and persistence model forecast values for January 20, 2017.

As for the iterative process, first the number of neurons was held constant at 10, and the delay parameter was modified from 2 to 6. Then, the best delay was held constant and the number of neurons was changed from 5 to 20. To make a first approximation, the number of neurons was varied with a 5-neuron step size to detect in which range the most accurate number of neurons was. Next, whether it will be necessary to run further tests inside the established ranges will be determined by the obtained RMSE values for each number of neurons. Further detail about the methodology can be found in [44]. For these tests, the training dataset was arranged into input vectors containing the following information: season, time of day, and the last 24 hrs of recorded temperature data in 10-minute intervals, whereas the forecaster's output is temperature value 10 min ahead. Although other meteorological parameters such as solar irradiation or wind speed are usually taken into account in developing forecasters for greater prediction horizons such as days or months [52], other studies in the literature claim that for very short-term horizons the correlation among these parameters is weak and unstable [44,51], and for those reasons endogenous forecasters are developed [53,54]. The results obtained through this methodology for the definition of the structure are presented in Table 1.

From Table 1 we concluded that there is little variation among the obtained RMSE values for those tests where the number of neurons was analysed, so it is not necessary to run further tests within these intervals

Table 1
Averaged results for fixing the structure of the RNN forecaster in Vitoria-Gasteiz, Basque Country.

Test number	Delay	Neurons	Training RMSE (°C)	Validation RMSE (°C)
1	1:2	10	0.2576	0.2652
2	1:3	10	0.2730	0.2819
3	1:4	10	0.2583	0.2657
4	1:5	10	0.2692	0.2780
5	1:6	10	0.2645	0.2722
6	1:2	5	0.2618	0.2688
7	1:2	15	0.2568	0.2648
8	1:2	20	0.2591	0.2670

to find the optimal number of neurons. In addition, the best architecture for temperature forecasting through an RNN was a 1:2 delay and 15 hidden neurons. Therefore, with this optimised RNN structure, training and validation RMSEs were 0.2568 °C and 0.2648 °C, respectively. This represents an improvement of 11.93% and 11.65% over the RMSEs that were set by the persistence benchmark. Fig. 4 compares the actual measurements and those obtained through the RNN model.

An analysis of Fig. 4 illustrates how sometimes the prediction value is sometimes lower and other times higher than the actual value. In contrast to the persistence model, the difference does not rely on the assumption that the predicted value for the chosen forecast horizon is equal to the last measured value. In this and the following MLP and SVM forecasters, the deviation between actual and predicted values relies on the fact that when sudden changes occur, the forecasters are not able to predict them accurately.

Fig. 5 shows the network layout developed by the RNN model, where W and b are the connection weights and bias, respectively. Both parameters and the internal loop for data retrofitting are characteristic of this model. It is possible to check how the data introduced by the loop is affected by the fitted delay function while the input data is not affected by the time delay function.

In addition, Table 2 lists the relevant aspects of the most accurate RNN forecaster's structure.

Multilayer perceptron network

Due to their characteristics, RNNs are not only more complicated to fix and optimise but they are also slower to train if they are compared against MLPs. In this study, several MLP architectures were checked to analyse whether the obtained results were more accurate than those of the RNNs. As there is no feedback loop in MLPs, it is not necessary to fix a delay parameter. Therefore, in order to obtain the most accurate forecaster, these tests consisted of modifying the number of hidden neurons. The Levenberg-Marquardt algorithm was applied in the training step due to its robustness and the accurate results achieved in other forecasters, [49,50,51].

As no methodology for fixing the number of neurons in the hidden layer was found in the literature, some sensitivity analyses were run. The number of hidden neurons between different structures was modified from 5 to 25 in 5-neuron intervals as proposed by [36,44]. Each architecture was run five times to avoid the effect of the random initialisation introduced by MATLAB®; the average results of these tests are shown in Table 3. For these tests, the input vectors contain the following information: season, time of day, and the last 24 hrs of recorded temperature data in 10-minute intervals, whereas the forecaster's output is temperature value 10 min ahead. After analysing the results presented in Table 3, we concluded that the structure with 15 neurons minimises the RMSE error metric for both training and validation datasets.

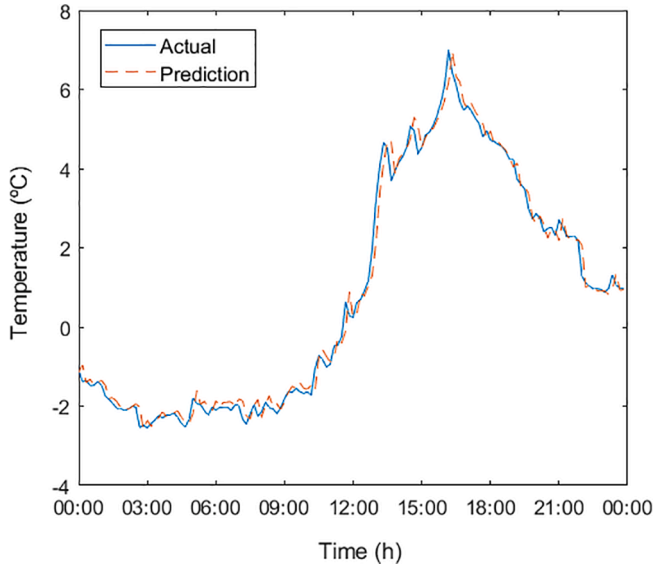

Fig. 4. Actual and RNN model forecast values for January 20, 2017.

We compared the optimal RNN and MLP structures and concluded that the latter's forecasts outperformed the former's. In an analysis of the training RMSEs for both forecasters, the MLP's value of 0.2515 °C was lower than the RNN's value of 0.2568 °C, which means an improvement of 2.06%. With respect to the validation RMSEs, the MLP architecture's value was 0.2618 °C while the RNN architecture's value was 0.2648 °C, which is an improvement of 1.13%. When the results were compared against persistence models, an improvement of 13.75% and 12.62% was obtained for training and validation forecasting accuracy, respectively. The actual measurements and those obtained through the MLP model are compared in Fig. 6.

Fig. 7 shows the network layout developed by the MLP model, where W and b are the connection weights and bias, respectively. Both parameters are characteristic of this model. It is possible to check how in this model there is no internal loop, due to the fact that in a MLP data is managed forward, from input to output without any loops.

In addition, Table 4 lists the relevant aspects of the most accurate MLP forecaster's structure.

Support vector machines

As Table 5 shows, different SVMs were implemented through MATLAB®. Previous studies that have developed SVMs for air temperature forecasting [39,42] have shown that certain parameters must be fixed, namely kernel functions and solvers. For that reason, in this study different combinations were analysed in order to select the optimal one. As in the previous cases, each of the combinations in Table 5 was tested five times and the RMSEs were averaged. For these tests, input vectors contain the following information: season, time of day, and the last 24 hrs of recorded temperature data in 10-minute intervals, whereas the forecaster's output is temperature value 10 min ahead.

The results presented in Table 5 show that the linear kernel function combined with the Sequential Minimal Optimisation had the lowest training and validation RMSE, 0.2761 °C and 0.2840 °C, respectively. The actual measurements and those obtained through the most accurate SVM model are compared in Fig. 8.

Even though these values are slightly less accurate than the values for the two ANN forecasters, they continue to be more accurate than the persistence model. With respect to the persistence benchmark, the training and validation RMSEs represent an improvement of 5.32% and 5.21%, respectively. This decrease in accuracy can be explained by the unsuitability of the kernel functions implemented for this problem. SVMs rely on fitting equations coefficients through databases to make predictions, making them less flexible than ANN forecasters in predicting previously unseen values or situations of sudden change. In addition, Table 6 lists the relevant aspects of the most accurate SVM forecaster's structure.

Finally, Table 7 summarises the best results obtained by each single method examined. The calculated values for the R^2 error metric in the validation step were also added.

N-nearest station model

An analysis of the results presented in Table 7 showed that there is not too much difference among models when the R-squared parameter is examined. The R-squared parameter analyses the whole amount of noise that we have in a given signal, so it can be concluded that all models have similar prediction abilities. However, if the RMSE metric is analysed, it can be seen that the MLPs made the best predictions for both the training and validation databases. The RMSE parameter analyses the

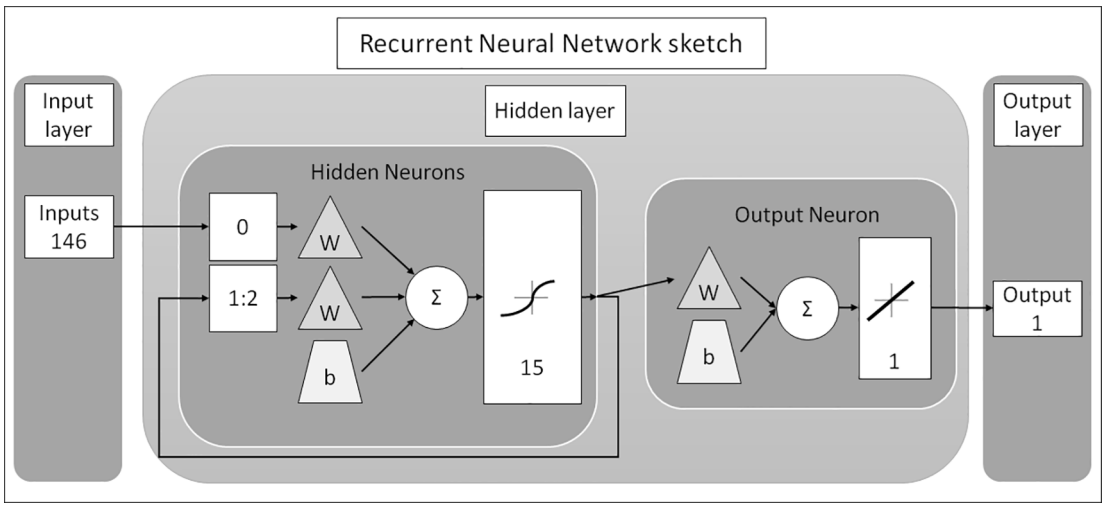

Fig. 5. Recurrent Neural Network's layout.

Table 2
Overview of the most accurate RNN structure.

Characteristics	RNN structure
Network type	Layer recurrent
Inputs (146)	Season, time, temperature
Outputs (1)	Temperature
Number of layers (3)	Input, hidden, output
Structure	Delay (1:2), Hidden Neurons (15), Output Neurons (1)
Functions	Log-sigmoid (hidden layer), Linear (output layer)
Training algorithm	Levenberg-Marquardt

Table 3
Averaged results for fixing the structure of the MLP forecaster in Vitoria-Gasteiz, Basque Country.

Test number	Neurons	Training RMSE (°C)	Validation RMSE (°C)
1	5	0.2536	0.2619
2	10	0.2517	0.2619
3	15	0.2515	0.2618
4	20	0.2518	0.2629
5	25	0.2517	0.2630

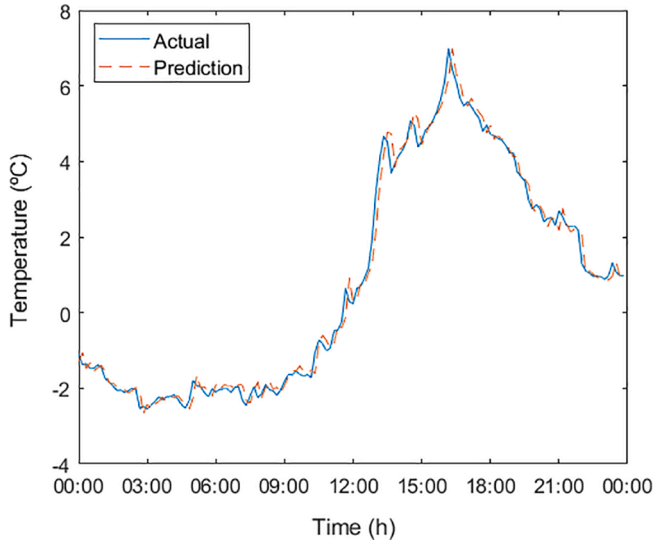

Fig. 6. Actual and MLP model forecast values for January 20, 2017.

deviation between each actual value and its prediction. Therefore, the specific, sudden changes which the model is not able to predict cause an increase in the RMSE parameter, as can be seen in SVM model.

Although there is a slight difference in accuracy for the RNN and MLP models, implementing the algorithm and making predictions have a lower computational cost in the MLP because of the lack of feedback loops. Therefore, this optimised MLP model was selected for the proposed forecaster, the N-nearest station model. To select the optimal forecaster, different tests were run, modifying the number of surrounding stations.

In this model, the input vectors were constructed in the same way as in the single station models. While in single station models the input vectors contain "season", "time of day" and the previous 24 h in 10-minute intervals for the target station, in the N-nearest model the input vectors contain not only the single station model's parameters but also the distance and relative position between the target and 'n-stations', and the last 24 h in 10-minute intervals for the temperature at those 'n' locations; the forecaster's output is the temperature value 10 min ahead.

As with the single station models, the training dataset was taken from 2015 to 2016 and the validation dataset was taken from the whole of 2017. Because there is not a method for selecting the optimal number of nearest stations and in order to minimise MATLAB's random initialisation, each test was repeated five times and the results were averaged in order to choose the most accurate option. Table 8 presents the averaged results obtained through this model.

After analysing the results in Tables 8, we concluded that while the lowest RMSE for training was obtained by the 10-nearest stations, the lowest RMSE for validation was obtained through the 6-nearest stations. Given that the prediction capacity of a forecaster is tested by the validation step because previously unseen values are used, for this study we selected the 6-nearest station model in order to develop the final forecaster. In addition, it was also determined from the results shown in Table 8 that, when the number of N-nearest stations is larger than in the optimal structure, the accuracy of the forecaster reduces. This decrease in accuracy relies on the fact that the greater the number of stations, the farther they are from the target location, thereby increasing the uncertainty of the proposed forecaster and diminishing its accuracy.

If the optimised forecaster's RMSEs are compared against those for persistence, an improvement of 20.44% and 13.22% can be seen in the training and validation datasets, respectively. With regard to the comparison with the MLP model, an improvement of 7.75% and 0.69% can be seen on the training and validation datasets, respectively. The R^2 error metric calculated in the validation step for the selected final architecture of the forecaster was 0.9986. From the results, we concluded that the proposed methodology, in which the information from the

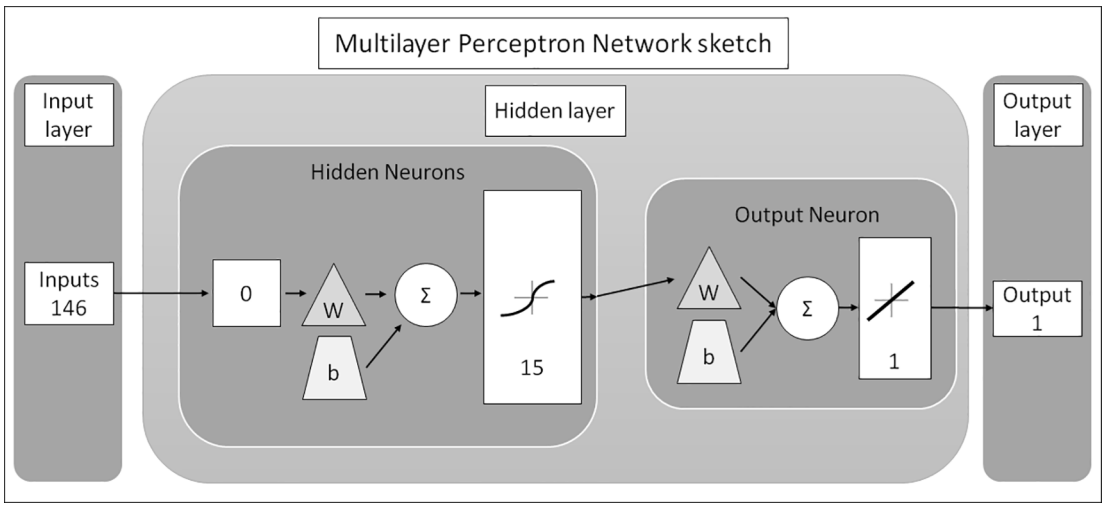

Fig. 7. Multilayer Perceptron Network's layout.

Table 4
Overview of the most accurate MLP structure.

Characteristics	MLP structure
Network type	Feedforward net
Inputs (146)	Season, time, temperature
Outputs (1)	Temperature
Number of layers (3)	Input, hidden, output
Structure	Hidden Neurons (15), Output Neurons (1)
Functions	Log-sigmoid (hidden layer), Linear (output layer)
Training algorithm	Levenberg-Marquardt

Table 5
Averaged results obtained for the different SVM alternatives in Vitoria-Gasteiz, Basque Country.

Solver	Kernel function	Training RMSE (°C)	Validation RMSE (°C)
Sequential Minimal Optimisation (SMO)	Linear	0.2761	0.2840
	Gaussian	0.4119	1.0292
	Radial basis	0.4074	0.9794
	Polynomial	0.4755	0.5217
Iterative Single Data Algorithm (ISDA)	Linear	0.2769	0.2847
	Gaussian	0.4060	0.9660
	Radial basis	0.4100	1.0082
	Polynomial	0.4976	0.5217

stations around the target location is used to make the predictions, slightly surpasses the traditional MLP forecaster, where information from only the target location is used. Therefore, it is up to the user's knowledge and the application's resolution requirements whether the traditional or proposed methodology is to be used. Nevertheless, the main limitation of this methodology is the need for a huge amount of data around the desired location in order to train the proposed forecaster. Fig. 9 shows a comparison between actual measurements and those obtained through the 6-nearest stations model.

In addition, Fig. 10 shows the network layout developed by the N-nearest station model, where W and b are the connection weights and bias, respectively. Both parameters are characteristic of this model.

To obtain the mathematical expression of the proposed model, Table 9 lists the relevant information for the developed N-nearest station model.

Using the information shown in Table 9 and the model's layout presented in Fig. 10, the forecaster's mathematical expression will be obtained starting from output and getting back to the system's inputs. Hence, the forecaster's output $\hat{o}$ is expressed as a mathematical linear

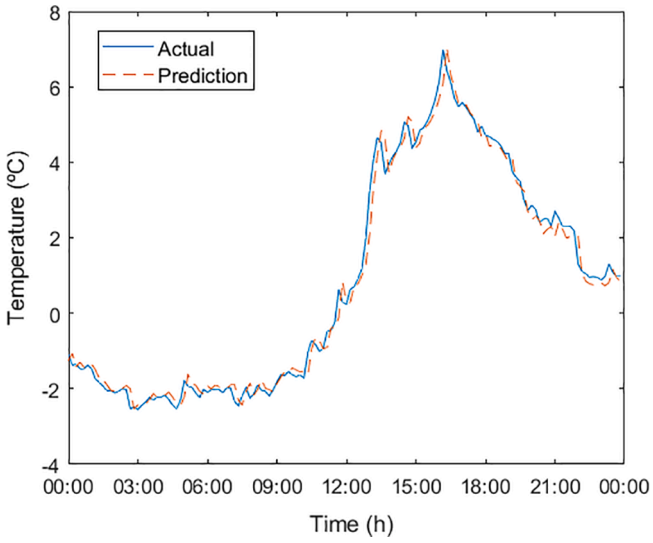

Fig. 8. Actual and SVM model forecast values for January 20, 2017.

Table 6
Overview of the most accurate SVM structure.

Characteristics	SVM structure
Solver	SMO
Kernel function	Linear
Inputs (146)	Season, time, temperature
Outputs (1)	Temperature

Table 7
Summary of the best error metrics obtained by each forecaster.

Test number	Training RMSE (°C)	Training improve (%)	Validation RMSE (°C)	Validation improve (%)	R^2 val.
Persistence	0.2916	–	0.2996	–	0.9981
RNN	0.2568	11.93	0.2648	11.65	0.9985
MLP	0.2515	13.75	0.2618	12.62	0.9985
SVM	0.2761	5.32	0.2840	5.21	0.9982

Table 8
Averaged results obtained for the new 'N-nearest stations' alternatives in Vitoria-Gasteiz, Basque Country.

Test number	'N-stations'	Training RMSE (°C)	Validation RMSE (°C)
1	5	0.2363	0.2622
2	6	0.2320	0.2600
3	7	0.2304	0.2665
4	8	0.2272	0.2707
5	10	0.2237	0.2744
6	15	0.2259	0.2941
7	20	0.2372	0.3233

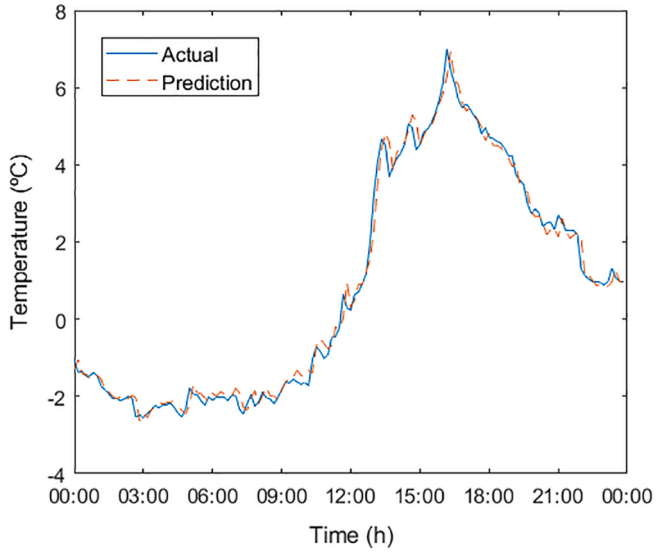

Fig. 9. Actual and N-nearest model forecast values for January 20, 2017.

combination of the hidden layer's neurons outputs,

$$\widehat{o} = \sum_{hn=1}^{HN} w_{hn,ON} y_{hn} + b_{OB}. \tag{8}$$

where $w_{hn,ON}$ represents each link between the output neuron and the hidden layer's neurons; b_{OB} refers to the output neuron's bias value and y_{hn} is thehn -th hidden layer's neuron output, which is represented as,

$$y_{hn} = j\left(\sum_{i=1}^{I} w_{i,hn}[p]_{i,1} + b_{hn}\right) \tag{9}$$

where j represents the sigmoid function used in hidden layer neurons, p is an array which contains the 1022 input values, $w_{i,hn}$ is the link values between the system's inputs and the hidden layer's neurons and b_{hn} is the bias value of the nh-th neuron. Therefore, by combining Eqs. (8) and (9), the proposed N-nearest station model is mathematically expressed as,

$$\widehat{o} = \sum_{hn=1}^{HN} w_{hn,ON} j\left(\sum_{i=1}^{I} w_{i,hn}[p]_{i,1} + b_{hn}\right) + b_{ON}. \tag{10}$$

In Fig. 11, a solid black square marks the target location where the temperature is going to be forecast; the white circles represent the available meteorological stations that have temperature databases that could be used to develop the forecaster proposed in this study, and the grey triangles indicate the location of the stations that were selected after the optimisation step for the proposed methodology had been carried out.

To identify the stations selected through the proposed methodology in Fig. 11 more easily, Table 10 shows the longitude and latitude coordinates of the chosen stations. These coordinates were used to calculate the distance and relative position between the target and 'n-stations'. As can be seen in Fig. 11, there are some stations close to the target location that there were not selected for the final forecaster. This

Table 9
Main characteristics of forecasters developed N-nearest station model.

Parameter	Value
Inputs (I)	1022 – season (1), time (1), distance and relative position between target location (6 * 2 = 12) and surrounding stations and target location's and surrounding stations' temperature data (144 * 7 = 1008)
Outputs ($\widehat{o}$)	1 – temperature
Number of Layers	3 – input, hidden, output
Number of Hidden Neurons (HN)	15
Number of Output Neurons (ON)	1
Number of Hidden Bias (HB)	15
Number of Output Bias (OB)	1

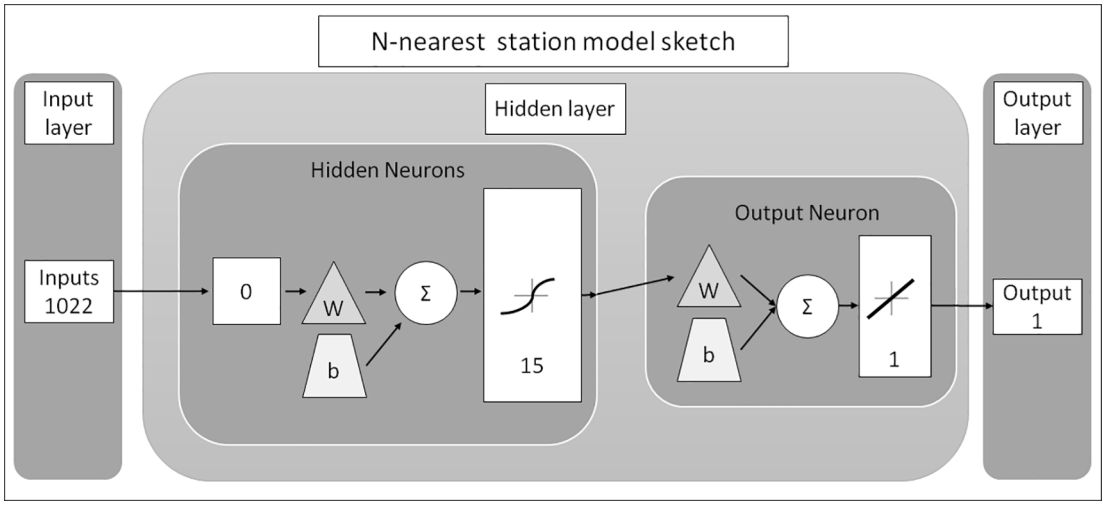

Fig. 10. Layout of N-nearest station model.

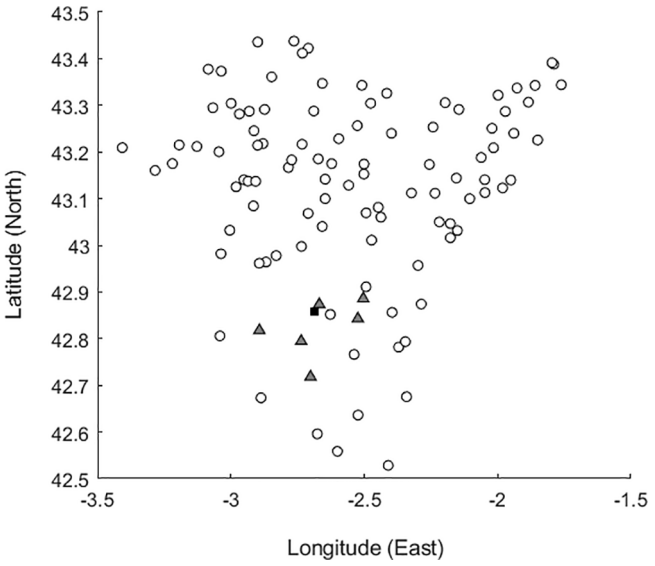

Fig. 11. Distribution of target (solid black square), selected (grey triangles) and available (white circles) meteorological stations.

Table 10
Relative distance and coordinates of the chosen stations.

Station	'Code'	Longitude (°)	Latitude (°)
Target	'C040'	42.85	−2.68
Stations chosen for the developed forecaster	'C076'	42.87	−2.66
	'C070'	42.79	−2.73
	'C020'	42.71	−2.70
	'C056'	42.84	−2.52
	'C049'	42.81	−2.89
	'C0AA'	42.88	−2.50

decision was supported by the fact that temperature databases in those stations were not properly recorded and there was missing information.

Moreover, we decided to analyse the accuracy of the developed forecaster on a day-by-day basis to check the deviation, in percentage, between the actual and forecasted values. Fig. 12 presents a pie chart diagram showing how throughout 2017 the accumulated deviation between the actual and predicted values throughout an entire day is less than 1% in 96.60% of examined samples. Furthermore, the mean value of this deviation was 0.2629%, thereby demonstrating that the accuracy of the forecaster is high enough to use for calculating solar power parameters.

With respect to the related literature, Yesilbudak et al. [55] suggested using curve fitting methods to forecast air temperature for a 10-minutes-ahead horizon. Yesilbudak et al. examined the accuracy of three methods denoted as Fourier, sum of sines and smoothing spline. While

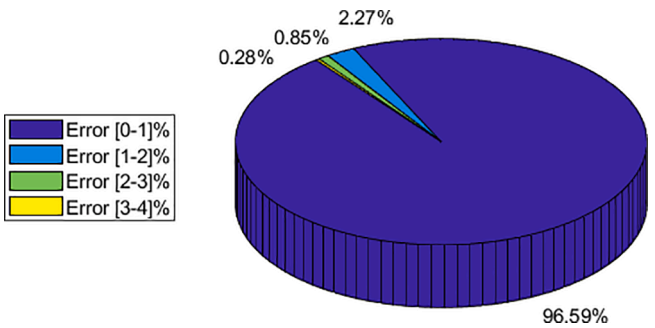

Fig. 12. Pie chart diagram of temperature forecasting error analysis for 2017.

the RMSE associated with each forecaster was 2.35 °C, 1.29 °C and 0.1824 °C, respectively, the R^2 values were 0.8046, 0.9403 and 0.9995. If both studies are compared, it can be concluded that the forecaster developed in this study is more accurate than at least the Fourier and sum of sines curve fitting methods.

With respect to the smoothing spline method, although it seems to surpass the accuracy of the forecaster developed here, Yesilbudak et al. do not predict new air temperature values outside the database that they used to fit the curve. Therefore, it can be concluded that smoothing spline is the proper method for fitting a forecast curve for a given database, but the accuracy of the method was not demonstrated for previously unseen temperature values.

Once we concluded that the model developed in this study slightly improves the accuracy of other forecasters available in literature, some simulations were run to demonstrate the model's suitability in computing photovoltaic generator key control parameters. To ensure proper monitoring and develop new control strategies, parameters such as cell temperature (T_c), open voltage circuit (V_{oc}), short circuit current (I_{sc}) and output power (P_m) must be calculated. While T_c, V_{oc} and I_{sc} are commonly used for control strategy purposes [2,47], P_m data is required by a network's operator to guarantee the quality of power supply or load following [19]. Photovoltaic generation involves mainly two meteorological parameters, solar irradiation and ambient temperature. While T_c and V_{oc} are strongly affected by ambient temperature, I_{sc} is mainly affected by solar irradiation [2] and P_m is affected by both. Therefore, a solar irradiation forecaster is also needed to compute these solar photovoltaic generators' key control parameters. However, several studies that address the goal of predicting solar irradiation for very short-term prediction horizon with great accuracy can be found in the literature [23,44]. Figs. 13–15 demonstrate how using the developed forecaster, the solar irradiation forecaster proposed by Rodriguez et al. [44] and equations proposed by Ayvazoğluyüksel et al. [2] make it possible to compute the T_c, V_{oc} and P_m solar photovoltaic control parameters.

Conclusions

The aim of this study consisted of developing a forecaster in a specific area, namely Vitoria-Gasteiz, Basque Country, that is able to predict outdoor temperature with a very short-term horizon, next 10 min, in order to compute the key control parameters of solar photovoltaic generators. The key conclusions from this study are as follows:

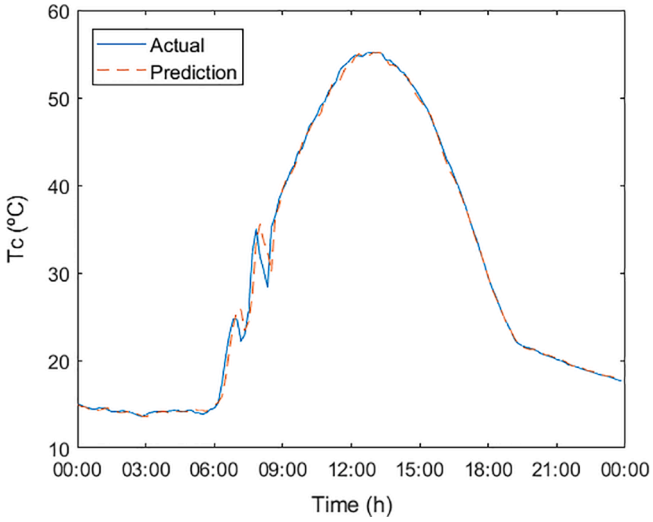

Fig. 13. Simulation of actual and forecasted T_c parameter in °C.

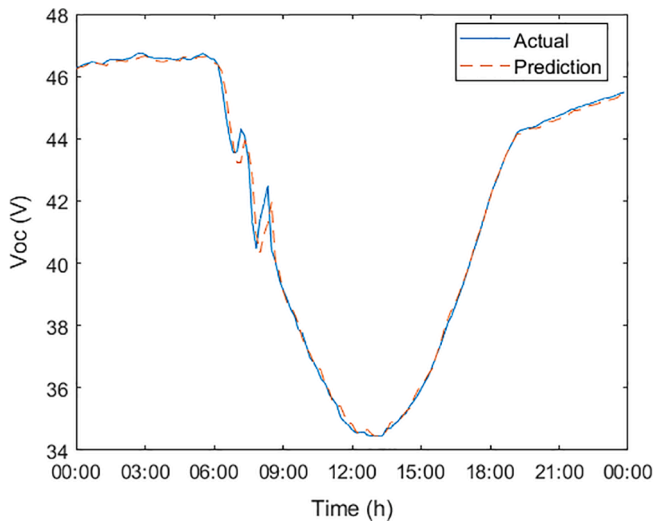

Fig. 14. Simulation of actual and forecasted V_{oc} parameter in V.

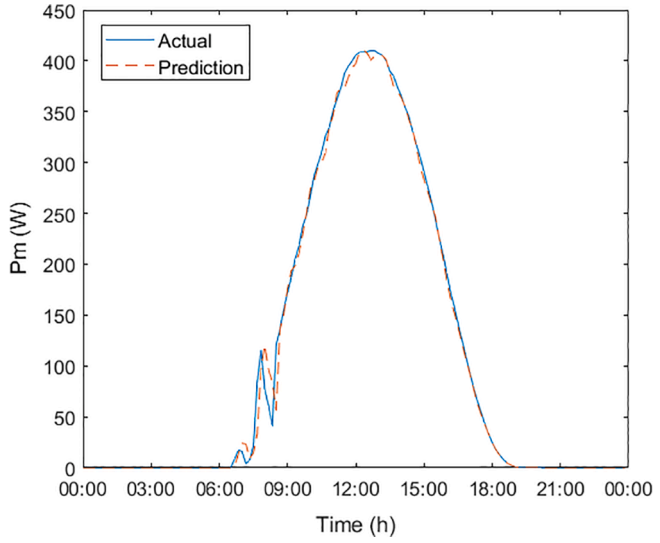

Fig. 15. Simulation of actual and forecasted P_m parameter in W.

- An analysis of the results obtained from the computed techniques shows that there is not much difference among models when the R^2 error metric is examined, all results being in the range of 0.9981 and 0.9985. Nevertheless, if the RMSE is examined, it can be concluded that the MLP technique has better accuracy for both training and validation databases, the result being 0.2515 °C and 0.2618 °C, respectively.
- The MLP structure was combined with the "N-nearest stations" method and that combined model was used to develop the tool presented in this study. Through the optimisation, it was concluded that optimal number of meteorological stations for this forecaster was six. With regards to the error metrics obtained by the most accurate configuration, the RMSE in the training and validation steps were 0.2320 °C and 0.26 °C, respectively. If these values are compared against the persistence benchmark, an improvement of 20.44% and 13.22% is achieved, respectively. The obtained R^2 value is 0.9986.
- The main drawback of this study is that both the methodology and the accuracy of the final forecaster was checked with real temperature measurements for 2017 in a specific location, Vitoria-Gasteiz, Basque Country. Even though it was demonstrated that the combined forecaster is more accurate than the single methods, it must be kept in mind that if this methodology were used in a different place, it would be necessary to fix the number of neurons of the MLP and the number of optimal stations. An additional challenge consists of obtaining the big databases required to develop or replicate the methodology presented in this paper. Finally, the forecaster's prediction horizon is limited due to the available databases' resolution sampling time, 10 min. Therefore, the forecaster's horizon cannot be lower than 10 min without manipulating the databases.
- The results presented here demonstrate that this temperature forecaster is useful for computing key control parameters for solar photovoltaic generators in the near future. However, our future studies will analyse the model's prediction accuracy when other parameters such as solar irradiation or wind speed are forecasted. It also will be interesting to perform some sensitivity analyses where the structure of the forecaster and the input window length are both examined to optimise the structure and reduce the computational cost. In addition, if temperature databases of other locations were available, it would be interesting to do some work toward the development of a universal method, based on the methodology proposed in this paper.

CRediT authorship contribution statement

Fermín Rodríguez: Conceptualization, Methodology, Validation, Resources, Investigation, Writing - original draft. **Michael Genn:** Methodology, Software, Resources, Investigation. **Luis Fontán:** Formal analysis, Supervision, Writing - review & editing. **Ainhoa Galarza:** Conceptualization, Visualization, Writing - review & editing.

Declaration of Competing Interest

The authors declare that they have no known competing financial interests or personal relationships that could have appeared to influence the work reported in this paper.

Acknowledgements

The authors would like to thank the Basque Government's Department of Education for financial support through the Researcher Formation Programme; grant number PRE_2019_2_0035.

References

[1] Afroz Z, Urmee T, Shafiullah, et al. Real-time prediction model for indoor temperature in a commercial building. Appl Energy 231: 2018; 29–53. 10.1016/j.apenergy.2018.09.052.
[2] Ayvazoğluyüksel Ö, Filik ÜB. Estimation methods of global solar irradiation, cell temperature and solar power forecasting: a review and a case study in Eskişehir. Renew Sustain Energy Rev 2018;91:639–53. https://doi.org/10.1016/j.rser.2018.03.084.
[3] Lotta MC, Pye S, Dodds PE. Quantifying the co-impacts of energy sector decarbonisation on outdoor air pollution in the United Kingdom. Energy Policy 2017;101:42–51. https://doi.org/10.1016/j.enpol.2016.11.028.
[4] Li S, Feng K, Li M. Identifying the main contributors of air pollution in Beijing. J Clean Prod 2017;163:359–65. https://doi.org/10.1016/j.jclepro.2015.10.127.
[5] Kibria A, Akhundjanov SB, Oladi R. Fossil fuel share in the energy mix and economic growth. Int Rev Econo Finan 2019;59:253–64. https://doi.org/10.1016/j.iref.2018.09.002.
[6] Teke A, Yıldırım HB, Çelik Ö. Evaluation and performance comparison of different models for the estimation of solar radiation. Renew Sustain Energy Rev 2015;50:1097–107. https://doi.org/10.1016/j.rser.2015.05.049.
[7] Barreto RA. Fossil fuels, alternative energy and economic growth. Econo Mod 2018;75:196–220. https://doi.org/10.1016/j.econmod.2018.06.019.
[8] REN21. The first decade: 2004–2014, 10 years of renewable energy progress; 2014. http://www.ren21.net/Portals/0/documents/activities/Topical%20Reports/REN21_10yr.pdf (accessed 10 December 2019).
[9] Rosales-Asensio E, Borge-Diez D, Blanes-Peiró JJ, et al. Review of wind energy technology and associated market and economic conditions in Spain. Renew Sustain Energy Rev 2019;101:415–27. https://doi.org/10.1016/j.rser.2018.11.029.

[10] Aguilar S, Telles GR, Medina P, et al. Wind power generation: a review and a research agenda. J Cleaner Prod 2019;218:850–70. https://doi.org/10.1016/j.jclepro.2019.02.015.
[11] Sahoo AK, Sahoo SK. Energy forecasting for grid connected MW range solar PV system. 7th India international conference on power electronics (IICPE); 2016. 10.1109/IICPE.2016.8079388.
[12] Che J, Wang J. Short-term load forecasting using a kernel-based support vector regression combination model. Appl Energy 2014;13:602–9. https://doi.org/10.1016/j.apenergy.2014.07.064.
[13] [13] European Union and Fuel Cell and Hydrogen Joint Undertaking; 2015. https://www.fch.europa.eu/sites/default/files/CommercializationofEnergyStorageFinal_3.pdf (accessed 13 January 2020).
[14] European Union and International Renewable Energy Agency (IRENA). Renewable Energy Prospects for the European Union; 2018. https://www.irena.org/-/media/Files/IRENA/Agency/Publication/2018/Feb/IRENA_REmap_EU_2018.pdf (accessed 10 January 2020).
[15] Renewable Energy Agency (IRENA); 2019. https://www.irena.org/-/media/Files/IRENA/Agency/Publication/2019/Feb/IRENA_Innovative_ancillary_services_2019.pdf?la=en&hash=F3D83E86922DEED7AA3DE3091F3E49460C9EC1A0 (accessed 14 January 2020).
[16] Attyaa AB, Anaya-Larab O, Leithead WE. Novel concept of renewables association with synchronous generation for enhancing the provision of ancillary services. Appl Energy 2018;229:1035–47. https://doi.org/10.1016/j.apenergy.2018.08.068.
[17] Donga J, Attyab AB, Anaya-Lara O. Provision of ancillary services by renewable hybrid generation in low frequency AC systems to the grid. Elec Pow Energy Syst 2019;105:775–84. https://doi.org/10.1016/j.ijepes.2018.09.017.
[18] Banshwar A, Sharma NK, Sood YR, et al. Renewable energy sources as a new participant in ancillary service markets. Energy Strat Rev 18: 2017; 106–120. 10.1016/j.esr.2017.09.009.
[19] Elsinga B, van Sark WGJHM. Short-term peer to peer solar forecasting in a network of photovoltaic systems. Appl Energy 2017;206:1464–83. https://doi.org/10.1016/j.apenergy.2017.09.115.
[20] Singh SN, Mohapatra A. Repeated wavelet transform based ARIMA model for very short-term wind speed forecasting. Renew Energy 2019;136:758–68. https://doi.org/10.1016/j.renene.2019.01.031.
[21] Bouzgou H, Gueymard CA. Fast short-term global solar irradiance forecasting with wrapper mutual information. Renew Energy 2019;133:1055–65. https://doi.org/10.1016/j.renene.2018.10.096.
[22] Qing X, Niu Y. Hourly day-ahead solar irradiance prediction using weather forecasts by LSTM. Energy 2018;148:461–8. https://doi.org/10.1016/j.energy.2018.01.177.
[23] Lopes FM, Silva HG, Salgado R, et al. Short-term forecast of GHI and DNI for solar energy systems operation: assessment of the ECMWF integrated forecasting system in southern Portugal. Sol Energy 2018;170:14–30. https://doi.org/10.1016/j.solener.2018.05.039.
[24] İlseven E, Göl M. Medium-term electricity demand forecasting based on MARS. IEEE PES innovative smart grid technologies conference Europe (ISGT-Europe); 2017. 10.1109/ISGTEurope.2017.8260124.
[25] Carvallo JP, Larsen PH, Sanstad AH, et al. Long term load forecasting accuracy in electric utility integrated resource planning. Energy Policy 2018;119:410–22. https://doi.org/10.1016/j.enpol.2018.04.060.
[26] Red Eléctrica de España (REE). Las energías renovables en el sistema eléctrico español; 2017. https://www.ree.es/sites/default/files/11_PUBLICACIONES/Documentos /Renovables-2017.pdf (accessed 13 December 2019).
[27] Mattei M, Notton G, Cristofari et al. Calculation of the polycrystalline PV module temperature using a simple method of energy balance. Renew Energy 31: 2006; 553–67. 10.1016/j.renene.2005.03.010.
[28] Kurtz S, Withfield K, Miller D, et al. Evaluation of high temperature exposure of rack-mounted photovoltaic modules. 34th IEEE photovoltaic specialist conference (PVSC); 2009. 10.1109/PVSC.2009.5411307.
[29] Curceac S, Ternynck C, Ouarda TBMJ, et al. Short-term air temperature forecasting using nonparametric functional data analysis and SARMA models. Environ Mod Soft 2019;111:394–408. https://doi.org/10.1016/j.envsoft.2018.09.017.
[30] Zhang X, Tan SC, Li G. Development of an ambient air temperature prediction model. Energy Build 2014;73:166–70. https://doi.org/10.1016/j.enbuild.2014.01.006.
[31] Papantoniou S, Kolokotsa DD. Prediction of outdoor air temperature using neural networks: application in 4 European cities. Energy Build 2016;114:72–9. https://doi.org/10.1016/j.enbuild.2015.06.054.
[32] Liu N, Babushkin V, Afshari A. Short-term forecasting of temperature driven electricity load using time series and neural network mode. J Clean Energy Tech 2014;2:327–31. https://doi.org/10.7763/JOCET.2014.V2.149.
[33] Mohammadi K, Shamshirband S, Danesh SS, et al. Temperature-based estimation of global solar radiation using soft computing methodologies. Theo Appl Clima 125: 2016; 101–112. 10.1007/s00704-015-1487-x.
[34] Paulescu M, Paulescu E, Gravila P, et al. Weather Modeling And Forecasting of PV systems operation. Springer; 2013. p. 17–42. 10.1007/978-1-4471-4649-0.
[35] Wang L, Lee EWM, Yuen RKK. Novel dynamic forecasting model for building cooling loads combining an artificial neural network and an ensemble approach. Appl Energy 2018;228:1740–53. https://doi.org/10.1016/j.apenergy.2018.07.085.
[36] Mba L, Meukam P, Kemajou A. Application of artificial neural network for predicting hourly indoor air temperature and relative humidity in modern buildings in humid region. Energy Build 2016;121:32–42. https://doi.org/10.1016/j.enbuild.2016.03.046.
[37] Li X, Zhao T, Zhang J. Prediction control for indoor temperature time-delay using Elman neural network in variable air system. Energy Build 2017;154:545–52. https://doi.org/10.1016/j.enbuild.2017.09.005.
[38] Li Q, Meng Q, Cai J, et al. Applying support vector machine to predict air cooling load in the building. Appl Energy 2009;86:2249–56. https://doi.org/10.1016/j.apenergy.2008.11.035.
[39] Ortiz-García EG, Salcedo-Sanz S, Casanova-Mateo C, et al. Accurate local very-short term temperature prediction based on synoptic situation Support Vector Regression banks. Atmos Resear 2012;107:1–8. https://doi.org/10.1016/j.atmosres.2011.10.013.
[40] Shumway RH, Stoffer DS. Time series analysis and its applications. 4th ed., New York; 2017. https://www.stat.pitt.edu/stoffer/tsa4/tsa4.pdf (accessed 8 December 2019).
[41] Dayhoff JE, DeLeo JM. Artificial neural networks. conference on prognostic factors and staging in cancer management: contributions of artificial neural networks and other statistical methods, Arlington; 1999. https://acsjournals.onlinelibrary.wiley.com/doi/full/10.1002/1097-0142%2820010415%2991%3A8%2B%3C1615%3A%3AAID-CNCR1175%3E3.0.CO%3B2-L (accessed 8 December 2019).
[42] Goodfellow I, Bengio Y, Courville A. Deep Learning. Cambridge, Massachusetts: MIT Press; 2016. https://www.deeplearningbook.org (accessed 23 November 2019).
[43] Haykin S. Neural networks and learning machines. Pearson Education, 3rd ed., Upper Saddle River New Jersey; 2009. http://dai.fmph.uniba.sk/courses/NN/haykin.neural-networks.3ed.2009.pdf (accessed 13 December 2019).
[44] Rodríguez F, Fleetwood A, Galarza A, et al. Predicting solar energy generation through artificial neural networks using weather forecast for microgrid control. Renew Energy 2018;126:855–64. https://doi.org/10.1016/j.renene.2018.03.070.
[45] Balluff S, Bendfeld J, Krauter S. Short term wind and energy prediction for offshore wind farms using neural networks. IEEE international conference on renewable energy research and applications (ICRERA); 2015. 10.1109/ICRERA.2015.7418440.
[46] Afroz Z, Urmee T, Shafiullah GM, et al. Real-time prediction model for indoor temperature in a commercial building. Appl Energy 2018;231:29–53. https://doi.org/10.1016/j.apenergy.2018.09.052.
[47] Panchal G, Ganatra A, Kosta YP, et al. Behaviour analysis of multilayer perceptrons with multiple hidden neurons and hidden layers. Int J Comput Theory Eng 2011;3:332–7. https://doi.org/10.7763/IJCTE.2011.V3.328.
[48] [48] MathWorks. Understanding support vector machine regression; 2018. [Online]. Available. https://au.mathworks.com/help/stats/understanding-support-vector-machine-regression.html. (accessed 15 November 2019).
[49] Rana M, Koprinska I. Forecasting electricity load with advanced wavelet neural networks. Neurocomputing 2016;182:118–32. https://doi.org/10.1016/j.neucom.2015.12.004.
[50] Mellit A, Massi A. A 24-h forecast of solar irradiance using artificial neural network: application for performance prediction of a grid-connected PV plant at Trieste, Italy. Sol Energy 2010;84:807–21. https://doi.org/10.1016/j.solener.2010.02.006.
[51] Rodríguez F, Florez-Tapia AM, Galarza A, Fontán L. Very short-term wind power density forecasting through artificial neural networks for microgrid control. Renew Energy 2020;145:1517–27. https://doi.org/10.1016/j.renene.2019.07.067.
[52] Prieto JI, Martínez-García FC, García D. Correlation between solar irradiation and air temperature in Asturias, Spain. Sol Energy 2009;83:1076–85. https://doi.org/10.1016/j.solener.2009.01.012.
[53] Louzazni M, Mosalam H, Khouya A, Amechnoue K. A non-linear auto-regressive exogenous method to forecast the photovoltaic power output. Sust Energy Tech Assess 2020;38. https://doi.org/10.1016/j.seta.2020.100670.
[54] Haddad S, Mellit A, Benghanem M, Daffallah KO. NARX-based short-term forecasting of water flow rate of a photovoltaic pumping system. a case study. J Sol Energy Eng 2016;138:11004–6. https://doi.org/10.1115/1.4031970.
[55] Yesilbudak M, Colak M, Bayindir R, et al. Very-short term modelling of global solar radiation and air temperature data using curve fitting methods. IEEE 6th international conference on renewable energy research and applications (ICRERA); 2017. 10.1109/ICRERA.2017.8191233.